3-21-2014

Laser sintering of separated and uniformly distributed multiwall carbon nanotubes integrated iron nanocomposites

Dong Lin
Purdue University, donglin@purdue.edu

Chunghorng Richard Liu
Purdue University, cliu@purdue.edu

Gary J. Cheng
Purdue University, Birck Nanotechnology Center, gjcheng@purdue.edu

Laser sintering of separated and uniformly distributed multiwall carbon nanotubes integrated iron nanocomposites

Dong Lin, C. Richard Liu, and Gary J. Cheng

Citation: Journal of Applied Physics **115**, 113513 (2014); doi: 10.1063/1.4869214
View online: http://dx.doi.org/10.1063/1.4869214
View Table of Contents: http://scitation.aip.org/content/aip/journal/jap/115/11?ver=pdfcov
Published by the AIP Publishing

Laser sintering of separated and uniformly distributed multiwall carbon nanotubes integrated iron nanocomposites

Dong Lin,[1] C. Richard Liu,[1] and Gary J. Cheng[1,2,3,a)]
[1]*School of Industrial Engineering, Purdue University, West Lafayette, Indiana 47906, USA*
[2]*School of Mechanical Engineering, Purdue University, West Lafayette, Indiana 47906, USA*
[3]*Birck Nanotechnology Center, Purdue University, West Lafayette, Indiana 47906, USA*

(Received 12 January 2014; accepted 10 March 2014; published online 21 March 2014)

Uniform distribution of carbon nanotubes (CNTs) in metal matrix during additive manufacturing of nanocomposites is always a challenge since the CNTs tend to aggregate in the molten pool. In this study, Multiwall carbon nanotubes (MWNTs) were separated and distributed uniformly into iron matrix by laser sintering process. MWNTs and iron powders were mixed together by magnetic stir, coated on steel 4140 surface, followed by laser sintering. Due to the fast heating and cooling rate, the CNTs are evenly distributed in the metal matrix. The temperature field was calculated by multiphysics simulation considering size effects, including size dependent melting temperature, thermal conductivity, and heat capacity. The SEM, TEM, and XRD were used to understand the laser sintering of CNT integrated nanocomposites. The results proved the feasibility of this technique to synthesize MWNTS integrated metal matrix nanocomposites. © *2014 AIP Publishing LLC*. [http://dx.doi.org/10.1063/1.4869214]

I. INTRODUCTION

The need for light weight, high strength materials has been promoted by the invention of airplane.[1] The advantages of these materials lead to the improvement of fuel efficiency. Metal matrix nanocomposites (MMNCs) have been broadly applied in aerospace and automobile industries because of their improved elastic modulus, hardness, tensile strength, and wear resistance performance with light weight.[2] In the MMNCs, the strength and ductility are provided by metal matrix and the strength and stiffness are provided by the reinforcement of nanomaterials. Nanomaterials have been introduced into metal matrix by several methods, such as vacuum sintering,[3] mechanochemical method,[4] laser sintering,[5] and ball milling.[6]

The first discover of carbon nanotube (CNT) was by Iijima in 1991. Due to the near perfect structure of CNTs, they are one of the strongest materials known to human beings. Based on direct or indirect measurement of mechanical properties, CNTs have the strength of 5 times higher than carbon fibers and also hold a better elastic modulus.[7] Besides the excellent mechanical properties, CNTs also have superior electrical and thermal conductivities since their ballistic nature of conduction of electrons and phonons. Because of these advantages, CNTs using as reinforcements for composite materials have been attracted much attention.

In recent years, there have been remarkable achievements of improving mechanical properties in carbon nanotube reinforced polymer matrix. However, it is only a little advance in carbon nanotube reinforced MMNCs since these carbon nanotubes tend to be agglomerated because of the strong van der Waals attractive force. Laser deposition has been applied to integrate CNT into nickel matrix.[8] However, the CNTs are aggregated after laser treatment. It is still a challenge to separate CNTs in the metal matrix.

This paper introduces a laser additive manufacturing technique to integrate 1D nanomaterials multiwall carbon nanotubes (MWNTs) into iron matrix, in which the MWNTs were separated and uniformly distributed in the cross section. Nanomaterials are mixed with iron powders by magnetic stirring in the DI water using Polyvinyl alcohol (PVA) as the dispersing agent.[5,9] The mixed powders were coated on the substrate surface, which was mechanically polished.[10–12] The volume ratio of nanomaterials can be adjusted easily during mixing. Laser sintering process was performed in a N_2 gas filled chamber to protect the samples from oxidation. After laser sintering, nanomaterials were successfully integrated into the cross section of iron matrix.

II. EXPERIMENTAL METHODS

The experimental setup of integrating MWNTs (from Cheaptubes, Inc.) into iron matrix is shown in Figure 1. Micro-sized iron powder and MWNTs were mixed together in DI water by magnetic stirring. The suspension was prepared by mixing iron powder and MWNTs with 4 wt. % of polyvinyl alcohol (PVA).[5,11,13] Single MWNTs can be separated successfully by using PVA as dispersing agent.[5] Mixed powders were coated on AISI 4140 surface and the cross section of coating is shown in Figure 1(a). Laser sintering was carried out by a Nd:YAG laser system under continuous-wave mode, which is shown in Figure 1(b). The output laser power was 100 W, while the beam size was 0.8 mm. The scanning speed and step size were 2 mm/s and 0.25 mm, respectively. Laser sintering process was fulfilled in a glass chamber filled with N_2 gas in order to protect the samples from oxidation.[5] The melting temperature of MWNTs is estimated around 3925–3970 K, which is much higher than the melting temperature of iron (1810 K). At selected laser

a)Author to whom correspondence should be addressed. Electronic mail: gjcheng@purdue.edu

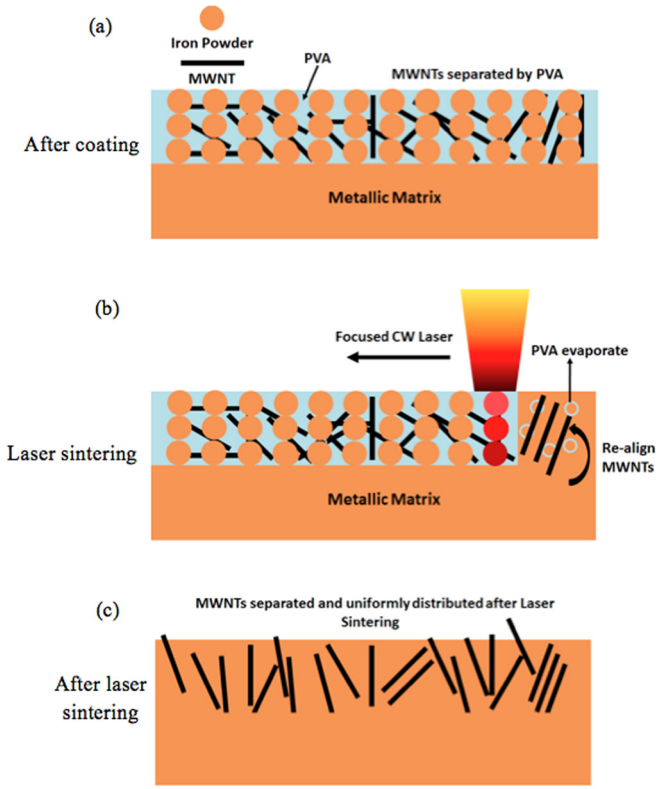

FIG. 1. Schematics of laser sintering of mixed iron powders with MWNTs. Cross-section of sample (a) after surface coating, (b) laser sintering process, and (c) after laser sintering.

intensity and scanning speed, the iron powders were melted while the MWNTs stayed solid[5] so that the MWNTs can be survived during laser sintering. During the laser irradiation, the PVA was evaporated from the melting pool of iron so that the laser sintered layer is PVA free.[5,9] The evaporation action of PVA bubbles helps to align the MWNTs in the melting pool. Heating and cooling rate in laser irradiation process is extremely fast ($\sim 10^{4-5}$ K/s).[2] Laser sintering process is too short for the MWNTs to be agglomerated together so that they can be still separated after laser sintering. Cross-sectional view after LS is represented in Figure 1(c). The coated layer was melted together with substrate during laser irradiation and the temperature field distribution will be discussed in detail by simulation results.

The substrates were low-alloyed steel AISI 4140 plate. These samples were first austenitized at 850 °C for 20 min and quenched by oil down to room temperature.[14] After austenitization, the samples were tempered at 450 °C for 2 h and naturally cooled down to room temperature in vacuum furnace. The hardness of samples after heat treatment is 310 VHN (Vickers hardness). The iron powder (average diameter of 4 μm), and MWNTs (outside diameter 8–15 nm) were selected for the coating.

Surface and cross sectional morphology were measured by Hitachi S-400 Field emission SEM. The material compositions before and after laser sintering were investigated by Bruker D8 Focus X-Ray diffractometer using Cu-Kα source. A FEI Nova 200 focused ion beam (FIB) system was used to prepare TEM samples by lift-out method. The microstructure images were obtained by the FEI Titan system operating at 300 keV. The surface hardness was measured by Leco M-400-H micro-hardness instrument with 300 g load and 10 s holding time.

III. RESULTS AND DISCUSSION

A. Temperature field simulation

The temperature field during laser sintering process was studied by Comsol Multiphysics with EM (electromagnetic) and HT (heat transfer) models.[11] The 2D model, which contains coated layer and substrate, was applied to investigate the temperature evolution by laser scanning. MWNTs were drawn vertically and uniformly distributed in the coated layer in order to simplify the simulation conditions. Temperature profiles of MWNTs and coated layer are the main concern of the simulation. The size and volume effect of nanomaterials on temperature profile were investigated.

1. Size dependent melting temperature

Understanding the thermal stability of single-walled carbon nanotubes (SWNTs) at high temperature is essential for the simulation of laser sintering process. SWNTs were thermally stable at 2800 °C in vacuum.[15] It was well established that the melting temperature of SWNTs is ~4450 K.[16] The Stone-Wales defects, intrinsic structure defects commonly existed in SWNTs, were 90° rotation of C-C bonds.[17,18] Premelting is existed in the defective region while this temperature is much lower than the melting temperature of the crystal.[19] Zhang *et al.*[15] simulated the melting temperature of perfect SWNTs and premelting of defective SWNTs. They found the melting occurred at a much smaller critical Lindemann parameter, $q_c = 0.03$, which was proposed for the clusters and homopolymers.[20] They used the parameter to calculate the melting temperature of perfect SWNTs and Stone-Wanes defects SWNTs,[15] which are 4800 K and 2600 K, respectively. The melting temperature range of MWNTs bought from Cheaptubes, Inc. is estimated from 3925 to 3970 K.

2. Size dependent thermal conductivity

It is still challenging to measure thermal conductivity by technological difficulties of synthesizing high-quality and well-ordered nanotubes.[21] Thus, it is essential to observe theoretical predictions of the thermal conductivity and the influence of various defects.[21] An unusually high thermal conductance should also be expected in carbon nanotubes, which are held together by sp^2 bonds.[22] The rigidity of these systems, combined with virtual absence of atomic defects or coupling to soft phonon modes of the embedding medium, should make isolated nanotubes very good candidates for efficient thermal conductors.[22]

Berber *et al.*[22] calculated the phonon thermal conductivity of isolated nanotubes. The phonon thermal conductivity of an isolated SWNT was investigated by theoretical calculation. At high temperatures, three-phonon Umklapp scattering begins to limit the phonon relaxation time.[23] Umklapp scattering requires production of a phonon beyond the Brillouin zone boundary because of the high Debye temperature of

diamond and graphite. The peak in the thermal conductivity of these materials is near 100 K, significantly higher than for most other materials.[23] The value of K at the peak (37 000 W/mK) is comparable to the highest thermal conductivity ever measured (41 000 W/mK for an isotopically pure diamond sample at 104 K). Even at room temperature, the thermal conductivity is quite high (6600 W/mK), exceeding the reported room temperature thermal conductivity of isotopically pure diamond by almost a factor of 2.[21,23] Sun *et al.* found that the thermal conductivity increased with increasing the length of the tube.[24] Che *et al.* investigated the relation between thermal conductivity and vacancy concentration and defect concentration.[21] Berber *et al.* used equilibrium molecular dynamics simulations based on the Green-Kubo expression that relates this quantity to the integral over time t of the heat flux autocorrelation function by[22,25]

$$\lambda = \frac{1}{3Vk_BT^2}\int_0^\infty \langle J(t)\cdot J(0)\rangle dt. \quad (1)$$

Here, k_B is the Boltzmann constant, V is the volume, T is the temperature of the sample and the angular brackets denote an ensemble average, and $J(t)$ is heat flux vector.

Kim *et al.*[26] found that thermal conductivity of a single MWNT is 3000 W/mK through measuring a microfabricated suspended device. Taking the volume-filling fraction of CNT's into account, the effective thermal conductivity for the MWNT's is about 2×10^2 W/mK.[27] The thermal conductivity of individual multi-walled carbon nanotubes by the 3-ω method at room temperature equals to 650–830 W/mK.[28] Aliev *et al.*[29] measured the thermal conductivity of single MWNTs of 10 μm electrode separation and the value was 600 ± 100 W/mK.

3. Size dependent specific heat capacity

The phonon structure of SWNTs at low temperature has been investigated by theoretical[30,31] and experimental efforts.[32] However, only few experiments have been conducted to measure the specific heat of bulk MWNT samples due to its complex structures.[33,34] The specific heat of millimeter long aligned MWNT bundles was indirectly measured by from 10 to 300 K.[33] Mizel *et al.*[34] found the behaviors of the low temperature specific heat for bulk MWNT and graphite were similar and they concluded it was from similar structures of the large radius MWNT and graphite. Theoretically calculation was also applied to calculate the low temperature specific heat of a 1–5 layered MWNT based on force constant dynamical models.[35] However, the theoretical values are different with the experimental data.[35] They found the specific heat data deviate from T^3 behavior at low temperature and fit needs additional T^{-2} term below 5 K, which is due to the nuclear hyperfine interaction of ferromagnetic impurities.

B. Simulation of temperature field during laser sintering

1. Temperature field of laser sintering coated iron layer on steel surface

The temperature profile of the sample during laser sintering was simulated in a 2D module, which can be seen in Figure 2. The height of coated layer and matrix were set as 50 μm and 2.35 mm, which were the real size of both layers. The width of the simulation model was set as 100 μm. The laser energy, beam size, and the scanning speed used in the simulation were 100 W, 0.8 mm, and 2 mm/s, respectively. The temperature distribution (at 0.28 s) in the cross section, without any MWNTs, is shown in Figure 2(a), while Figure 2(b) is the temperature profile in the coated layer. The maximum temperature at 0.28 s in the cross section is around 2010.5 K, which is much higher than the melting temperature of iron (1810 K), however, is much lower than the melting temperature of MWNTs. The minimum temperature in the coated layer is also higher than the melting temperature of substrate, thus providing the chance to melt coated layer together with matrix.

2. MWNTs size effect on temperature field during laser sintering

The size effect on temperature distribution is shown in Figure 3. The volume fraction was set as 2% and the outside

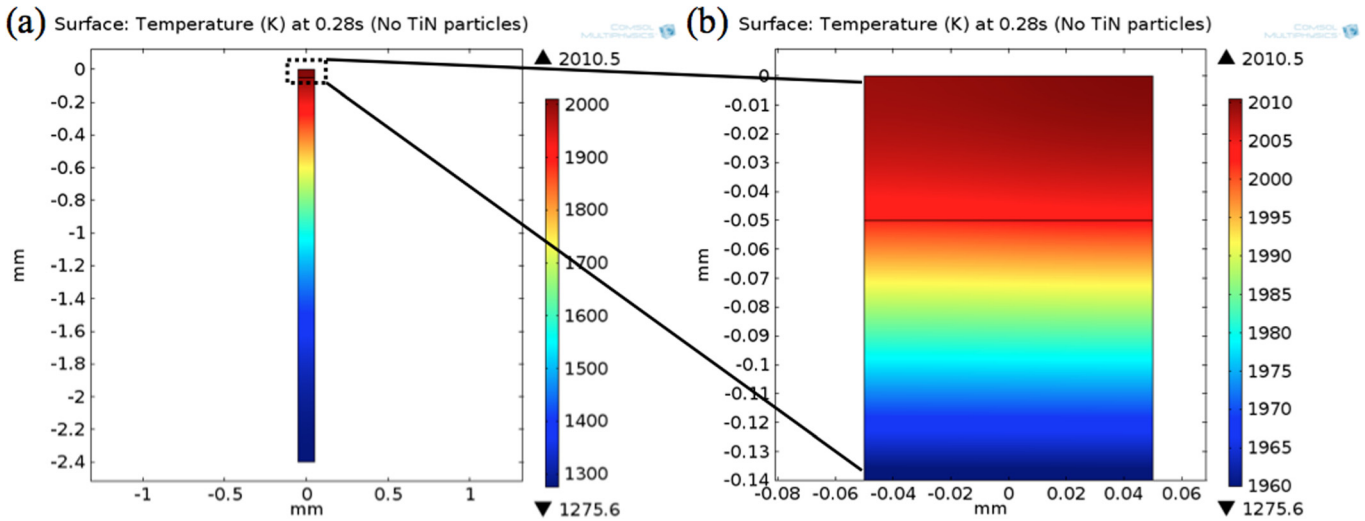

FIG. 2. Temperature distribution at the time of 0.28 s without MWNTs embedding in the (a) cross section and (b) coated layer.

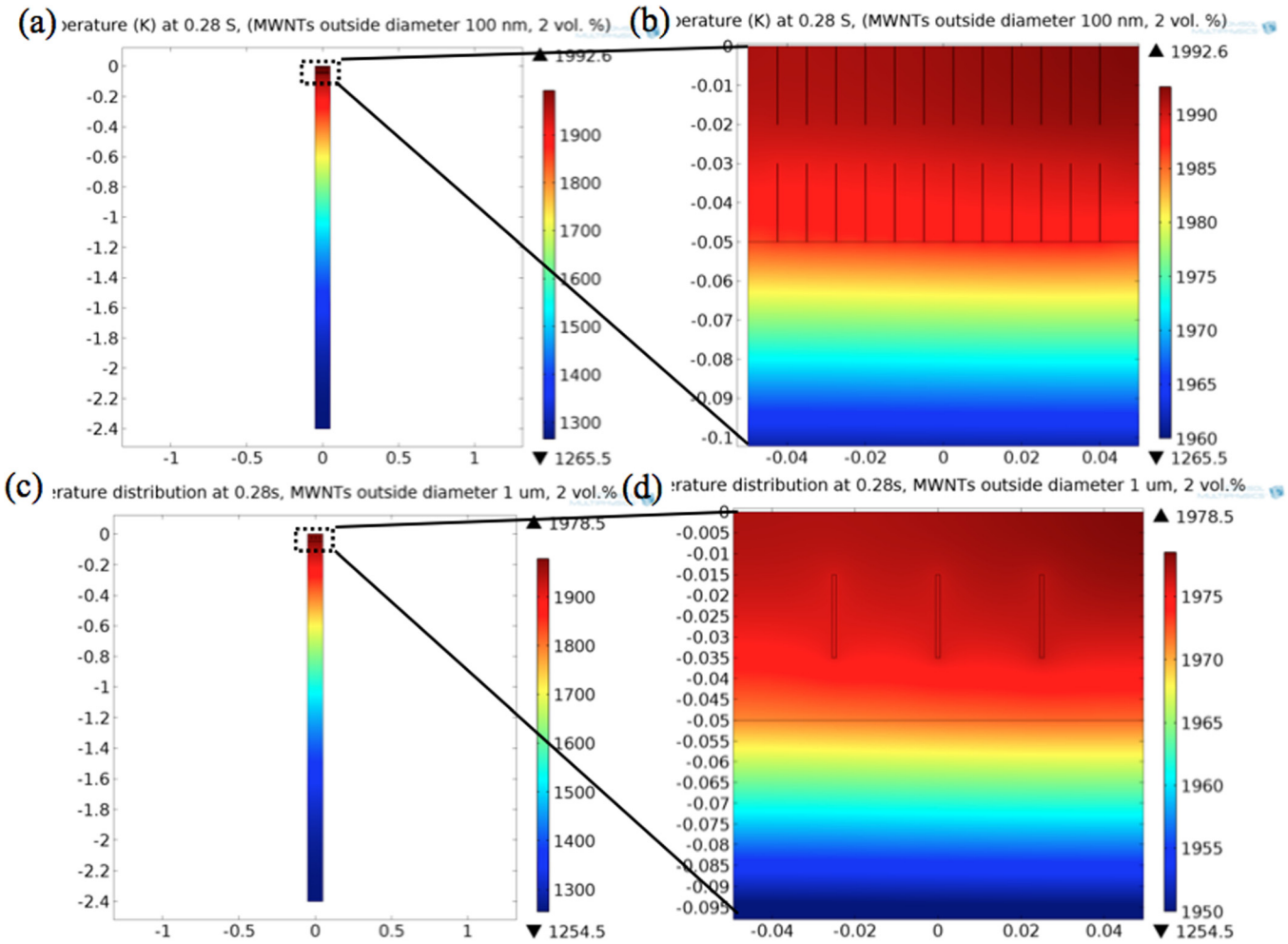

FIG. 3. Carbon nanotubes (2 vol. %) size effect on temperature field during laser sintering process (a) and (c): outside diameter of 100 nm and 1 μm, (b) and (d): temperature field in the coated layer of (a) and (c).

diameters of MWNTs were 100 nm (Figures 3(a) and 3(b)), and 1 μm (Figures 3(c) and 3(d)), respectively. The MWNTs were drawn to vertically and uniformly distribute in the cross section in order to simplify the simulation conditions. The maximum temperature of Figures 3(a) and 3(c) at 0.28 s are 1992.6 K and 1978.5 K. It shows that the maximum temperature decreases with increasing the outside diameter of carbon tubes. The temperature difference between maximum and minimum temperature of 100 nm and 1 μm are 727.1 K and 724.0 K. It represents that temperature distribution does not affected too much with the size of CNTs when the volume ratio is fixed. The temperature on both coated layers is higher than the melting point of iron, which means it is possible for the coated layer melting together with the matrix.

The temperature distribution around carbon tubes (outside diameter 1 μm) is shown in Figure 4. It only contains 3 carbon tubes since the outside diameter of carbon tubes is large. The temperature field around marked carbon tubes of A, B, and C are shown in Figures 4(b)–4(d), respectively. The bended temperature field is caused by the high thermal conductivity of carbon tubes. The thermal conductivity of carbon tubes was set as 6600 W/mK, which is much higher than iron matrix (300 W/mK). It conducts heat much faster than the iron matrix, which is also the reason for small temperature difference at both ends of carbon tubes when compared to nearby iron matrix.

3. WNTs volume effect on temperature field of laser sintering

The volume ratio effects on the temperature during laser irradiation were also studied. Figures 5(a) and 5(c) show the temperature distribution of 4 and 8 vol. % of MWNTs (outside diameter is 100 nm) at 0.28 s. These results demonstrate that the sample temperature decreases with increasing the volume ratio of MWNTs. Figures 6(b) and 6(d) show the temperature distribution on the coated layer at 0.28 s of Figures 6(a) and 6(c). The maximum temperatures, which is shown in Table I, of 0, 2 vol. %, 4 vol. %, and 8 vol. % are 2010.5 K, 1992.6 K, 1981.3 K, and 1926.2 K, respectively. Larger volume ratio of MWNTs shows better effect on heat conduction, since MWNTs have much larger thermal conductivity when compared to the iron matrix. The higher thermal conductivity helps decrease the temperature in the coated layer. The matrix also has a lower minimum temperature for higher volume ratio of carbon nanotubes.

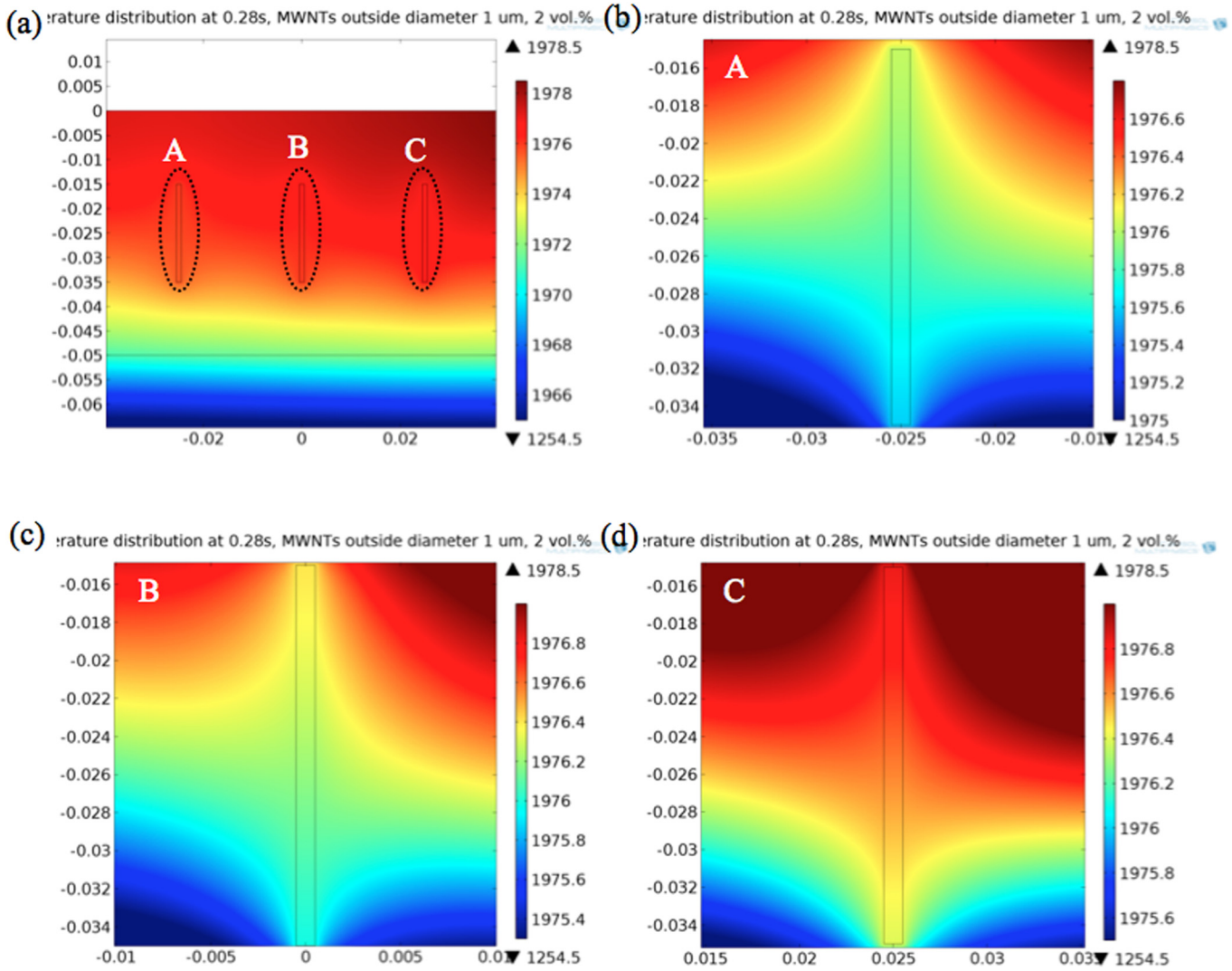

FIG. 4. (a) Temperature field distribution in the coated layer with 2 vol. % of carbon nanotubes (outside diameter 1 μm), (b), (c), and (d) temperature field around marked carbon tubes of A, B, and C.

C. LS process conditions

1. Microstructure after integrating MWNTs into iron matrix

When the interaction of laser radiation with metal powders occurs, the energy deposition is considered to be both bulk-coupling and powder-coupling mechanism.[13,36] During the first laser pulse, the energy is absorbed in a narrow layer of the powder particles. This layer has a higher temperature than other parts of the iron powder. The thickness of this layer is related to the thermal penetration depth, which is proportional to the square root of thermal diffusivity of the medium times time interval.[13] Then the temperature profile of iron powders tends to be uniform after many pulses and reaches to the melting temperature of iron powders. The maximum temperature of particle surface is reached at the end of one pulse[13]

$$\Delta T_{\max} = \frac{2AI_0}{k}\sqrt{\frac{\kappa_{th}\tau_p}{\pi}}, \tag{2}$$

where A is the absorptivity, I_0 is the intensity, k is the thermal conductivity, κ_{th} is the heat diffusivity, and τ_p is the laser pulse duration.

During laser sintering, the melting/solidification process is the only mechanism feasible for rapid bonding of metal powders.[37] Full melting was performed in order to meet the need of full dense objects, with mechanical properties comparable to those bulk materials and by the desire of further fatigue test.[13] The time needed for the temperature of whole particles to be uniform can be defined as

$$\Delta t_h \approx \frac{r^2}{\kappa_b}, \tag{3}$$

where r is the particle radius, which is around 2 μm and $\kappa_b \sim 2.3 \times 10^{-5}$ m^2/s. It takes $\Delta t_h \sim 0.17$ μs for the particles to be homogenization.

Multiple modes of mass, heat, and momentum transfer and chemical reaction would happen during laser sintering process.[38] The Marangoni effect occurs when the surface tension gradient is risen by the temperature gradient in the molten pool.[39] The surface of matrix was polished before coating since balling effect prefers to happen due to the oxide layer between coated layer and the matrix.[38] Former research pointed out that adding graphite for laser sintering iron powders provides following beneficial effect: increases

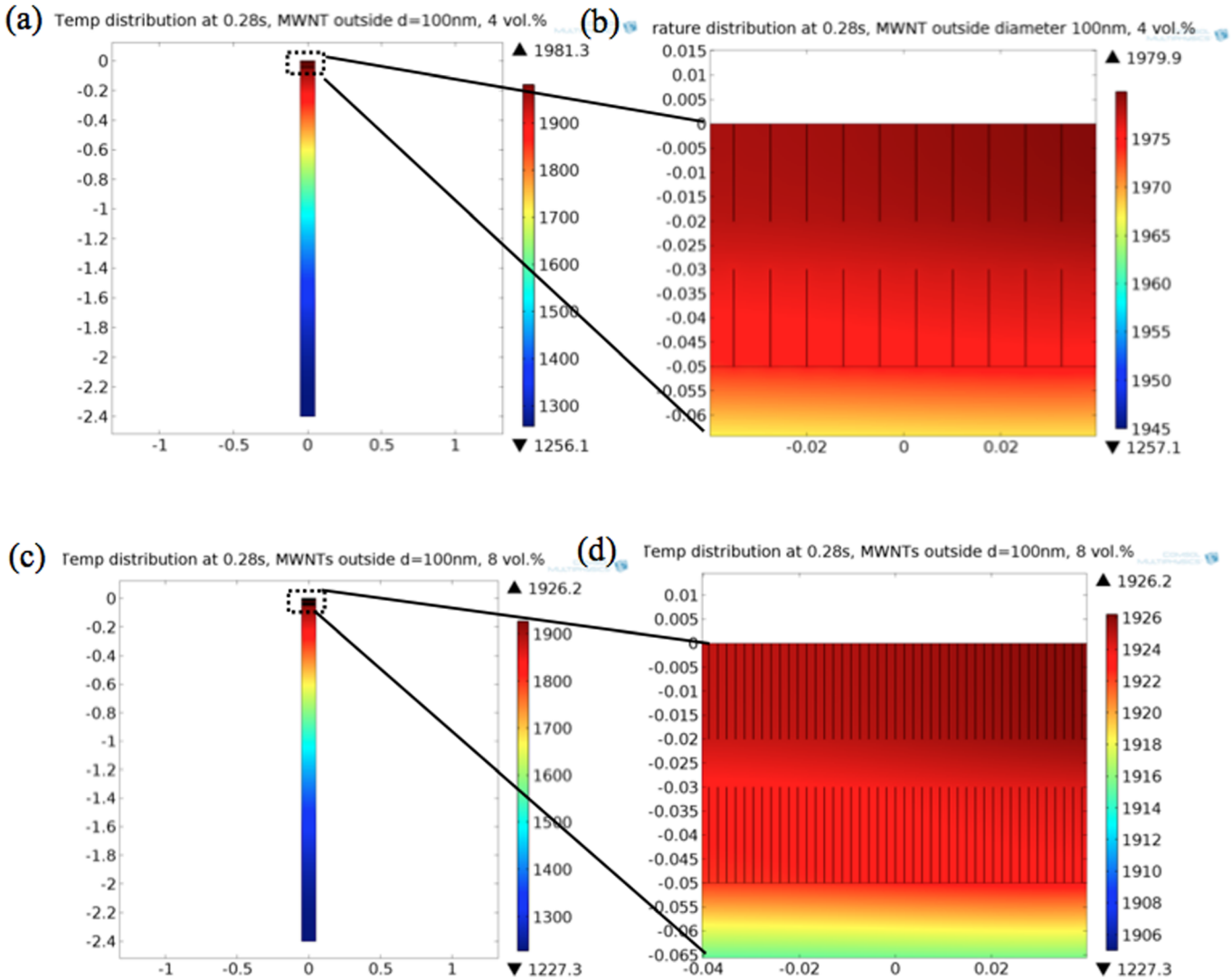

FIG. 5. MWNTs (outside diameter 100 nm) volume ratio effects on temperature field during laser sintering (a) and (b) 4 vol. % and 8 vol. % at 0.28 s, (c) and (d) temperature field distribution on the coated layer of (a) and (b).

the sintered density with increasing the graphite weight ratio, helps to avoid structure of pores, and decreases the surface roughness, etc.[11] The SEM image of surface morphology of laser sintered Fe/MWNTs nanocomposites is shown in Figures 6(a) and 6(b). The Nd:YAG laser system was operated at 100 W. The scanning speed was 2 mm/s and the step size was 0.25 mm. The MWNTs, which were survived from laser sintering, at surface are marked in Figures 6(a) and 6(b). The exposure of MWNTs outside may be caused by the evaporation of PVA. The evaporation process generates high density of bubbles and the escaping of bubbles would realign the MWNTs in the cross section. The MWNTs in the cross section are also represented by TEM image, which is shown in Figure 6(c). These MWNTs are separated and uniformly distributed in the iron matrix

Bubbles rise through a liquid are very popular in engineering practice, including chemical engineering, metallurgy, and especially in biotechnology.[40] The rising of gas bubbles has been investigated since the beginning of 19th century.[41] Many equations have been developed in order to calculate the rising velocity of gas bubbles in a liquid. Among these equations, the most reliable semiempirical equation is developed by Davies and Taylor[42]

$$U = 25V^{1/6}, \tag{4}$$

where V is the bubble volume. This equation only works for the case of large, spherical cap-shaped bubbles.[40] For a single isolated smallest bubbles, which are considered as perfect spheres, Stokes solution can be used to reasonably calculate the rising velocity[43]

$$U = \frac{1}{18}\frac{gd_e^2(\rho_l - \rho_g)}{\mu_l}, \tag{5}$$

where g is the gravity acceleration, d_e is the equivalent bubble diameter (diameter of a sphere with same volume as the bubble), μ_l is the dynamic viscosity of liquid, ρ_l is the density of liquid, and ρ_g is the density of gas.

The drag coefficient C_D of gas bubble is calculated based on the equivalent sphere diameter. The balance of forces acting on a rising bubble can be written as[40]

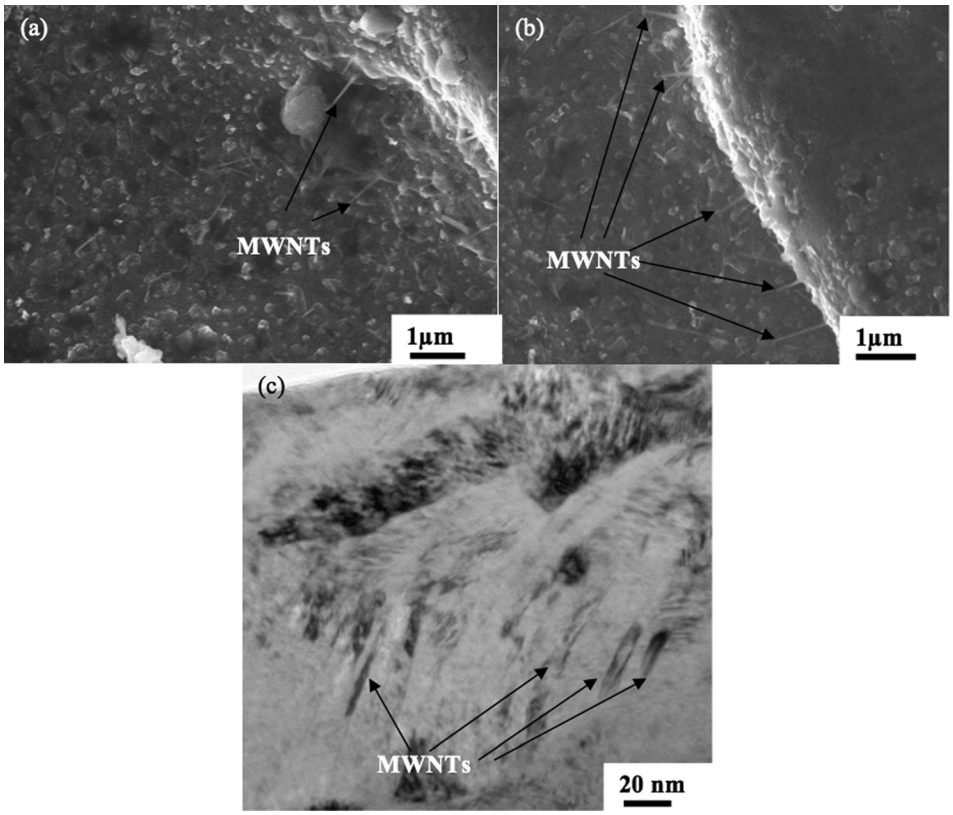

FIG. 6. (a) and (b) Surface morphology of Fe/MWNTs nanocomposites after laser sintering and (c) MWNTs distributed in the cross section of iron matrix.

$$\frac{1}{2}C_D S\rho_l U^2 = \Delta\rho g V, \tag{6}$$

where $\Delta\rho$ is the difference between the liquid and gas densities, $S = \pi d_h^2$, where d_h is the diameter projected on the horizontal plane circle and $V = \pi d_e^3/6$. Equation (5) can be rewritten as

$$C_D = \frac{4g\Delta\rho d_e^3}{3\rho d_h^2 U^2}. \tag{7}$$

The drag force generated during rising of PVA bubbles helps to realign the MWNTs vertically in the cross section of liquid iron in order to decrease the resistance for these bubbles to escape. It explains the vertically aligned MWNTs in the surface of laser sintered layer in Figure 6(c). The simulated temperature of top surface is much lower than the melting temperature of MWNTs, which is the reason for the MWNTs to be survived.

Figure 7 shows high resolution TEM image of a single MWNT in the iron matrix. It clearly exhibits graphene layers in the walls.[8] The diameter of the MWNT is around 8 nm based on the measurement of TEM image, which agrees with the information provided by the producer that the outside diameter of MWNT is between 8 and 15 nm. One single carbon nanotube existed in the iron matrix means that PVA was successfully separated MWNTs. It also proves that MWNTs survived during the laser sintering process and did not dissolve in the molten iron pool.[8] The interaction between SWNT or MWNT with matrix includes two manners: end contact and side contact.[7] End contact and side contact mean that metal matrix reacts with carbon nanotube at the end and the wall of nanotube, respectively.[7] It would be very strong leading to the formation of carbides through end contact by the sigma bond formation.[7] Weak interaction occurs in side contact condition through weak bond formed by out-of-plane orbitals.[7] The interface between the walls of carbon nanotube and iron shows no significant evidence of

TABLE I. Volume effects of carbon nanotubes on maximum and minimum temperature of the whole model.

Volume ratio	0	2 vol. %	4 vol. %	8 vol. %
Max temp (K)	2010.5	1992.6	1981.3	1926.2
Min temp (K)	1275.6	1265.5	1256.1	1227.3

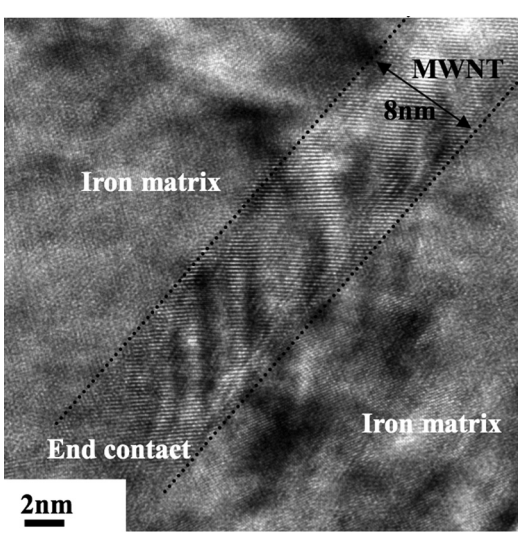

FIG. 7. One single MWNT integrated into iron matrix.

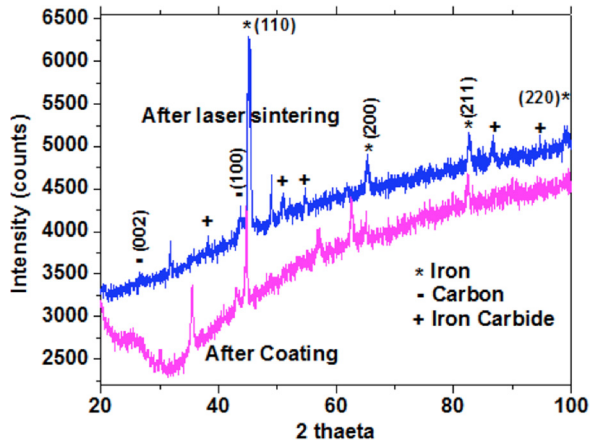

FIG. 8. XRD patterns of Fe/MWNTs after coating and laser sintering.

side contact. The MWNTs are rolled up graphene sheets and they only have the end carbon atoms with unsaturated covalent bonds.[8] The end side of MWNT in Figure 7 at the left bottom provides direct evidence of end reaction.

The formation of carbides due to reaction between CNT and the matrix could adversely alter the mechanical properties. If the volume ratio of the carbide is high enough (>5%), then one can observe peaks corresponding to the phase in the XRD pattern. XRD study of randomly oriented CNTs will result in the peak at $2\theta = 26°$ corresponding to the graphite (002) plane spacing = 0.34 nm.[44] XRD as such is not a confirmative technique for the presence of carbon nanotubes because the peaks are of graphite. However, the XRD can be used to detect different carbide peaks by a small scan rate of 0.05°/s. The existing carbon peaks of XRD further prove that carbon nanotubes survived during laser sintering (Figure 8).

2. Surface micro-hardness

Near surface work hardening is also measured under three conditions (Figure 9): as received, laser sintered 11 wt. % of TiN nanoparticle, and laser sintered of 2 wt. % MWNTs. The Vickers hardness of as received sample is 310 VHN. After laser sintering 11 wt. % TiN nanoparticles the surface hardness increases to 410 VHN, around 32% higher than original value. The surface hardness increases to 605 VHN when integrating with 2 wt. % MWNTs. It is about 95.2% increase from original sample. It clearly shows that MWNTs have much better surface hardness improvement than TiN nanoparticles.

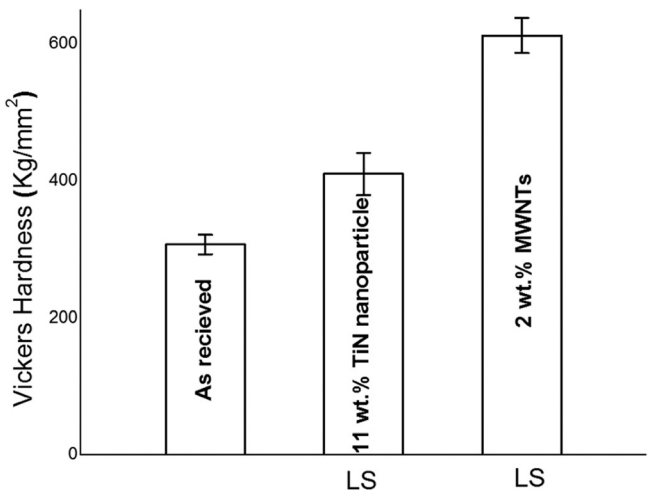

FIG. 9. Surface micro-hardness of as-received sample, embedding 11 wt. % TiN nanoparticles, and 2 wt. % of MWNTs by laser sintering.

IV. CONCLUSION

Laser assisted integrating MWNTs into iron matrix were investigated by experiment and simulation study. The simulation results show that volume ratio has a higher effect on the temperature field when comparing with the size of MWNTs. The temperature filed simulated by Comsol shows that MWNTs is possible to survive after laser sintering. The SEM, TEM, and XRD results confirmed the successful separating and integrating MWNTs into the iron matrix. The technique provides a strategy to integrate 1D nanomaterials into metal matrix.

ACKNOWLEDGMENTS

The authors appreciate the partially financial support from NSF grant (CMMI 0900327).

[1]S. Bakshi, D. Lahiri, and A. Agarwal, Int. Mater. Rev. **55**, 41 (2010).
[2]G. J. Cheng, D. Pirzada, M. Cai, P. Mohanty, and A. Bandyopadhyay, Mater. Sci. Eng. **25**, 541 (2005).
[3]Y. C. Luo and D. Y. Li, J. Mater. Sci. **36**, 4695 (2001).
[4]F. Shehata, A. Fathy, M. Abdelhameed, and S. F. Moustafa, Mater. Des. **30**, 2756 (2009).
[5]D. Lin, C. Ye, Y. L. Liao, S. Suslov, C. R. Liu, and G. J. Cheng, "Mechanism of fatigue performance enhancement in a laser sintered superhard nanoparticles reinforced nanocomposite followed by laser shock peening," J. Appl. Phys. **113**, 133509 (2013).
[6]E. Yarrapareddy and R. Kovacevic, Surf. Coatings Technol. **202**, 1951 (2008).
[7]S. R. B. A. Agarwal and D. Lahiri, *Carbon Nanotubes Reinforced Metal Matrix Composites* (CRC Press, 2011).
[8]J. Y. Hwang, A. Neira, T. W. Scharf, J. Tiley, and R. Banerjee, Scr. Mater. **59**, 487 (2008).
[9]D. Lin, C. Ye, S. Suslov, Y. Liao, C. R. Liu, and G. J. Cheng, in *Mechanism of Fatigue Performance Enhancement in a Superhard Nanoparticles Integrated Nanocomposites by a Hybrid Manufacturing Technique* (American Society of Mechanical Engineers, 2013), p. V001T01A051.
[10]D. Lin, M. Y. Zhang, C. Ye, Z. Liu, C. R. Liu, and G. J. Cheng, Appl. Surf. Sci. **258**, 4254 (2012).
[11]D. Lin, S. Suslov, C. Ye, Y. Liao, C. R. Liu, and G. J. Cheng, Appl. Surf. Sci. **258**, 2289 (2012).
[12]D. Lin, Y. Yang, and G. J. Cheng, Appl. Surf. Sci. **283**, 924 (2013).
[13]P. Fischer, V. Romano, H. P. Weber, N. P. Karapatis, E. Boillat, and R. Glardon, Acta Mater. **51**, 1651 (2003).
[14]C. Ye, S. Suslov, B. J. Kim, E. A. Stach, and G. J. Cheng, Acta Mater. **59**, 1014 (2011).
[15]Z. Kaiwang, G. M. Stocks, and Z. Jianxin, Nanotechnology **18**, 285703 (2007).
[16]S. Minomura, *Solid State Physics Under Pressure: Recent Advances with Anvil Devices* (Springer, 1985).
[17]A. J. Stone and D. J. Wales, Chem. Phys. Lett. **128**, 501 (1986).
[18]A. Hashimoto, K. Suenaga, A. Gloter, K. Urita, and S. Iijima, Nature **430**, 870 (2004).
[19]A. M. Alsayed, M. F. Islam, J. Zhang, P. J. Collings, and A. G. Yodh, Science **309**, 1207 (2005).
[20]Y. Zhou, M. Karplus, K. D. Ball, and R. S. Berry, J. Chem. Phys. **116**, 2323 (2002).
[21]C. Jianwei, Ç. Tahir, and A. G. William III, Nanotechnology **11**, 65 (2000).

[22]S. Berber, Y.-K. Kwon, and D. Tománek, Phys. Rev. Lett. **84**, 4613 (2000).
[23]J. Hone, *Carbon Nanotubes: Thermal Properties* (Marcel Dekker, 2004).
[24]K. Sun, M. A. Stroscio, and M. Dutta, J. Appl. Phys. **105**, 074316 (2009).
[25]A. A. A. T. Ramanathan, S. Stankovich, D. A. Dikin1, M. Herrera-Alonso, R. D. Piner, D. H. Adamson, H. C. Schniepp, X. Chen, R. S. Ruoff, S. T. Nguyen, A. Aksay, R. K. Prud'Homme, and L. C. Brinson, Nat. Nanotechnol. **3**, 327 (2008).
[26]P. Kim, L. Shi, A. Majumdar, and P. L. McEuen, Phys. Rev. Lett. **87**, 215502 (2001).
[27]D. J. Yang, Q. Zhang, G. Chen, S. F. Yoon, J. Ahn, S. G. Wang, Q. Zhou, Q. Wang, and J. Q. Li, Phys. Rev. B **66**, 165440 (2002).
[28]T. Y. Choi, D. Poulikakos, J. Tharian, and U. Sennhauser, Appl. Phys. Lett. **87**, 013108 (2005).
[29]E. A. Ali, H. L. Marcio, M. S. Edward, and H. B. Ray, Nanotechnology **21**, 035709 (2010).
[30]R. Saito, T. Takeya, T. Kimura, G. Dresselhaus, and M. S. Dresselhaus, Phys. Rev. B **57**, 4145 (1998).
[31]J. Yu, R. K. Kalia, and P. Vashishta, J. Chem. Phys. **103**, 6697 (1995).
[32]J. Hone, B. Batlogg, Z. Benes, A. T. Johnson, and J. E. Fischer, Science **289**, 1730 (2000).
[33]W. Yi, L. Lu, Z. Dian-lin, Z. W. Pan, and S. S. Xie, Phys. Rev. B **59**, R9015 (1999).
[34]A. Mizel, L. X. Benedict, M. L. Cohen, S. G. Louie, A. Zettl, N. K. Budraa, and W. P. Beyermann, Phys. Rev. B **60**, 3264 (1999).
[35]V. N. Popov, Phys. Rev. B **66**, 153408 (2002).
[36]C. B. Mo, S. I. Cha, K. T. Kim, K. H. Lee, and S. H. Hong, Mater. Sci. Eng. **395**, 124 (2005).
[37]A. Simchi and H. Pohl, Mater. Sci. Eng. **359**, 119 (2003).
[38]A. Simchi and H. Pohl, Mater. Sci. Eng. **383**, 191 (2004).
[39]L. Pawlowski, J. Therm. Spray Technol. **8**, 279 (1999).
[40]D. G. Karamanev, AIChE J. **40**, 1418 (1994).
[41]H. Allen, Philos. Mag. **50**, 323 (1900).
[42]R. Davies and G. Taylor, Proc. R. Soc. London Ser. A **200**, 375 (1950).
[43]G. G. Stokes, *Mathematical and Physical Papers, 1* (Cambridge University Press, 1880).
[44]S. R. B. A. Agarwal and D. Lahiri, *Carbon Nanotubes: Reinforced Metal Matrix Composites* (CRC Press, 2010).